THE JOURNAL OF BIOLOGICAL CHEMISTRY VOL. 289, NO. 41, pp. 28202–28212, October 10, 2014


# Tandem Pore Domain Halothane-inhibited $K^+$ Channel Subunits THIK1 and THIK2 Assemble and Form Active Channels*

Received for publication, July 28, 2014, and in revised form, August 13, 2014 Published, JBC Papers in Press, August 22, 2014, DOI 10.1074/jbc.M114.600437

**Sandy Blin[‡], Franck C. Chatelain[‡], Sylvain Feliciangeli[‡], Dawon Kang[§], Florian Lesage[‡1], and Delphine Bichet[‡]**

*From [‡]LabEx ICST, Institut de Pharmacologie Moléculaire et Cellulaire, CNRS, and Université de Nice Sophia Antipolis, 660 Route des Lucioles, 06560 Valbonne, France and the [§]Department of Physiology and Institute of Health Sciences, Gyeongsang National University, School of Medicine, Jinju 660-751, South Korea*

**Background:** THIK1 and THIK2 are related leak $K^+$ channel subunits.
**Results:** Assembly of THIK1 with THIK2 was shown by dominant negative effects of pore-mutated subunits, *in situ* proximity ligation assay, FRET, and electrophysiology of covalent THIK1/THIK2 dimers.
**Conclusion:** THIK1 and THIK2 assemble and form active channels.
**Significance:** In cell and tissues co-expressing THIK1 and THIK2, heterodimeric channels may contribute to cell excitability.

**Despite a high level of sequence homology, tandem pore domain halothane-inhibited $K^+$ channel 1 (THIK1) produces background $K^+$ currents, whereas THIK2 is silent. This lack of activity is due to a unique combination of intracellular retention and weak basal activity in the plasma membrane. Here, we designed THIK subunits containing dominant negative mutations ($THIK1^{DN}$ and $THIK2^{DN}$). $THIK2^{DN}$ mutant inhibits THIK1 currents, whereas $THIK1^{DN}$ inhibits an activated form of THIK2 (THIK2-A155P-I158D). *In situ* proximity ligation assays and Förster/fluorescence resonance energy transfer (FRET) experiments support a physical association between THIK1 and THIK2. Next, we expressed covalent tandems of THIK proteins to obtain expression of pure heterodimers. Td-THIK1-THIK2 (where Td indicates tandem) produces $K^+$ currents of amplitude similar to Td-THIK1-THIK1 but with a noticeable difference in the current kinetics. Unlike Td-THIK2-THIK2 that is mainly detected in the endoplasmic reticulum, Td-THIK1-THIK2 distributes at the plasma membrane, indicating that THIK1 can mask the endoplasmic reticulum retention/retrieval motif of THIK2. Kinetics and unitary conductance of Td-THIK1-THIK2 are intermediate between THIK1 and THIK2. Altogether, these results show that THIK1 and THIK2 form active heteromeric channels, further expanding the known repertoire of $K^+$ channels.**

Electrophysiology has identified many different native $K^+$ currents that have been classified according to the mechanisms or stimuli that control their activity. Then the cloning of the corresponding $K^+$ channels has shown that they form the largest family of ion channels with more than 78 genes encoding pore-forming subunits (1). These subunits are divided into three major classes according to their membrane topology. In the first class, $Ca^{2+}$-and $Na^+$-activated subunits ($K_{Ca}$, $K_{Na}$) are related to voltage-dependent ($K_v$) channels that have a central core with six transmembrane segments (TMS).[2] In the second class, inwardly rectifying, ATP-sensitive and G protein-coupled $K^+$ channel ($K_{ir}$) subunits have only two TMS. 6TMS and 2TMS subunits contain a single pore domain (P), and the assembly of four subunits is necessary to form a functional pore (2, 3). The leak or background $K^+$ channels ($K_{2P}$) with two pore domains (P1 and P2) per subunit form the last family. Two subunits containing four TMS assemble to form the ion conduction pathway (4, 5). Many pore-forming subunits form functional homomeric as well as heteromeric channels. Depending on the number of possible combinations, this heteromerization dramatically enhances the number of functionally distinct $K^+$ channels, providing the cells with an increased diversity of $K^+$ channels without increasing the number of genes (1).

Heteromerization occurs between closely related subunits and has been observed within almost all the different subfamilies of 6TMS and 2TMS proteins (6–14). In comparison, little is known about the assembly of $K_{2P}$ channels. Unlike KCNK7 and TASK5, which are silent subunits, all $K_{2P}$ channels produce functional homodimers (15–17). Few examples of heteromerization have been reported. The first example is well documented and relates to the TASK subfamily. Functional TASK1/TASK3 heterodimers present intermediate properties due to the different pharmacologies and pH sensitivities of the two individual subunits (18, 19). The second example concerns the potential dimerization of TWIK1 with TASK1 or TASK3 (20). TWIK1 would confer sensitivity to sumoylation to TWIK1/TASK heteromeric channels. Although the existence of such

* This work was supported by the Fondation pour la Recherche Médicale (Equipe labellisée FRM 2011) and by the Agence Nationale de la Recherche (Laboratory of Excellence "Ion Channel Science and Therapeutics" Grant ANR-11-LABX-0015-01).
[1] To whom correspondence should be addressed. Tel.: 33-4-93-95-77-27; Fax: 33-4-93-95-77-04; E-mail: lesage@ipmc.cnrs.fr.

[2] The abbreviations used are: TMS, transmembrane segments; THIK, tandem pore domain halothane-inhibited $K^+$ channel; Td, tandem; MDCK, Madin-Darby canine kidney; FRET, Förster/fluorescence resonance energy transfer; ROI, region(s) of interest; PLA, proximity ligation assay; PLC, phospholipase C; pS, picosiemens; EYFP, enhanced YFP; ECFP, enhanced CFP; DN, dominant negative; ER, endoplasmic reticulum; TASK, TWIK-related acid-sensitive $K^+$ channel.

dimers between members of distant subfamilies would be particularly original, it is still uncertain because of the controversial regulation of TWIK1 by small ubiquitin-like modifier (SUMO) (21, 22). Finally, the last and most recent example is the assembly of TWIK1 with TREK1 that produces astrocytic passive conductance and cannabinoid glutamate release from astrocytes (23).

Tandem pore domain halothane-inhibited $K^+$ channel 1 (THIK1) produces background $K^+$ currents (24). Despite 62% amino acid identity with THIK1 (KCNK13, $K_{2P}$13.1), THIK2 (KCNK12, $K_{2P}$12.1) is not active upon heterologous expression (24, 25). Previously, we have shown that this apparent lack of activity is due to a unique combination of strong retention in endoplasmic reticulum and low intrinsic channel activity at the plasma membrane (26). A THIK2 mutant containing a proline residue in its second membrane-spanning segment (THIK2-A155P) produces $K^+$-selective currents with properties similar to THIK1, including inhibition by halothane and insensitivity to extracellular pH variations (26). The cytoplasmic N-terminal region of THIK2 contains an arginine-rich motif that acts as a retention/retrieval signal. Mutation of this motif in THIK2 induces a relocation of THIK2 to the plasma membrane resulting in measurable currents. The same results were described using rat THIK subunits rather than the human ones (27). Altogether these results demonstrate that THIK2 is able to form active homodimers. Here, we show that THIK1 and THIK2 co-assemble and form functional channels in the plasma membrane.

## EXPERIMENTAL PROCEDURES

*Constructs*—Human THIK1 was cloned into the HindIII/XhoI sites of pLIN, a derivative of the pGEM vector for expression in *Xenopus* oocytes or pcDNA3 (Invitrogen), for expression in mammalian cells (Madin-Darby canine kidney (MDCK)). Human THIK2 was cloned into the HindIII/BamHI sites of pLIN and pCDNA3 vectors. To generate dominant negative THIK1 (G113E) and THIK2 (G132E) and hyperactive THIK2 channels (A155P-I158D), site-directed mutagenesis was carried out by PCR of the full-length plasmid by using PfuTurbo DNA polymerase (Agilent). The entire cDNAs were sequenced. Wild-type and mutated THIK1-THIK2 tandems were constructed by overlapping PCRs and cloned into HindIII/SalI sites of pLIN and HindIII/XhoI sites of pcDNA3 Zeo (−) (Invitrogen). THIK1-THIK1 and THIK2-THIK2 tandems were constructed by separate PCRs and cloned into XbaI-HindIII-SalI sites of pLIN and XbaI-HindIII-XhoI of pcDNA3. For immunocytochemistry experiments, Myc (EQKLISEEDL), HA (YPYDVPDYA), or V5 (GKPIPNPLLGLDST) tags were inserted by PCR at the N or C terminus of THIK1, THIK2, and TREK1. GIRK2-V188G is cloned into HindIII/XhoI sites of pLIN (28). For *in situ* proximity ligation assay and single-channel recordings, THIK1-Myc, TREK1-HA, THIK2-HA, THIK2-5RA-HA, and Td-THIK1-THIK2 were subcloned into pIRES2-EGFP vector (Invitrogen). For fluorescence resonance energy transfer experiments, THIK1 and THIK2 were subcloned into HindIII/BamHI sites of pECFP-N1 and pEYFP-N1. TREK1-EYFP was a generous gift from Dr Amanda Patel.

*Oocyte Expression and Two-electrode Voltage Clamp Recordings*—Capped cRNAs were synthesized by using the AmpliCap-Max T7 high yield message maker kit (CellScript) from plasmids linearized by AflII. RNA concentration was quantified using a NanoDrop (Thermo scientific). Stage V-VI *Xenopus laevis* oocytes were collected, injected with 1–10 ng of each cRNA, and maintained at 18 °C in ND96 solution (96 mM NaCl, 2 mM KCl, 2 mM $MgCl_2$, 1.8 mM $CaCl_2$, 5 mM Hepes, pH 7.4). Oocytes were used 1–3 days after injection. Macroscopic currents were recorded with two-electrode voltage clamp (Dagan TEV 200 or iTEV90 HEKA Elektronik amplifier). Electrodes were filled with 3 M KCl and had a resistance of 0.5–2 megaohms. A small chamber with a rapid perfusion system was used to change extracellular solutions and was connected to the ground with a 3 M KCl-agarose bridge. All constructs were recorded in ND96. Stimulation of the preparation, data acquisition, and analysis were performed using pClamp software (Molecular Devices) or PatchMaster (HEKA Elektronik). All recordings were done at 20 °C.

*MDCK Cell Expression and Immunocytochemistry*—MDCK cells were grown in 24-well plates on coverslips and transiently transfected with THIK plasmids using Lipofectamine 2000 (Invitrogen). 24–48 h after transfection, cells were fixed and permeabilized, and channels were labeled with primary anti-HA antibody (HA-7, Sigma, 1/1000) or anti-Myc antibody (9E10, Roche Applied Science, 1/1000), and secondary anti-mouse coupled to Alexa Fluor 488 (Invitrogen). To test for co-localization of THIK channels with plasma membrane or endoplasmic reticulum, an mCherryFP-PH-PLCδ plasmid was co-transfected to visualize the cell surface, or the cells were labeled with anti-calreticulin antibody (PA3-900, Thermo Scientific, 1/1000) and secondary anti-rabbit antibody coupled to Alexa Fluor 594 (Invitrogen). Coverslips were mounted in Mowiol medium onto slides and observed with a confocal microscope (LSM780 Carl Zeiss).

*Duolink Proximity Ligation Assay (PLA)*—Duolink *in situ* PLA probe anti-mouse PLUS (DUO92001), *in situ* PLA probe anti-rabbit MINUS (DUO92005), and Duolink *in situ* detection reagents red kit (DUO92008) were purchased from Sigma-Aldrich. MDCK cells were co-transfected with a pIRES2-EGFP and a pCDNA3 construct each containing a $K_{2P}$ subunit (0.5 μg each). Cells were fixed, permeabilized, and incubated with primary mouse anti-HA (HA-7, Sigma, 1/1000) or mouse anti-Myc (9E10, Roche Applied Science, 1/1000) and rabbit anti-V5 (PRB-189P, Covance, 1/1000) antibodies for 2 h at 37 °C in antibody diluent solution from kit. Cells were processed for Duolink revelation according to the manufacturer's recommendations. Finally, coverslips were mounted onto slides. Observation fields were randomly chosen using a Zeiss microscope with a 40× objective.

*Förster/Fluorescence Resonance Energy Transfer (FRET)*—FRET measurements were done on a laser scanning confocal microscope (TCS SP5, Leica Microsystems) using gradual acceptor photobleaching strategy (29). CFP and YFP images of the entire cells were sequentially taken during 2 min (40 sequences) using a 63×/1.4 NA oil immersion objective. CFP was excited at low power of the 405-nm laser to avoid direct excitation of YFP and photobleaching during acquisition. CFP

emission was detected between 430 and 496 nm. YFP was photobleached inside a region of interest (ROI) with full power laser at 514 nm, and images of this photobleaching were taken from 525 to 589 nm. To specifically measure FRET at the plasma membrane and to eliminate signal from the endoplasmic reticulum, ROI were chosen to only target the cell surface. 12-bit raw images were analyzed using a home-made ImageJ macro program (30). This macro analyzed the intensity variations of the CFP fluorescence emission inside the ROI where YFP was bleached. Three ROI on the CFP stack of images were used. First, a ROI of the YFP bleached area was defined for CFP measurement ($I_{measure}$). Another ROI of the background ($I_{background}$) was chosen to correct $I_{measure}$. $I_{measure}$ was also corrected for photobleaching induced by image acquisition using a third ROI ($I_{photo}$) inside the cell but apart from the first ROI. Mean gray values were extracted from each ROI, and the CFP intensity was corrected according to this formula

$$I_{corrected} = (I_{measure} - I_{background})/(I_{photo} - I_{background}) \quad \text{(Eq. 1)}$$

FRET efficiency was calculated using the following formula: $(I_{max} - I_0)/I_{max}$. $I_0$ corresponds to CFP intensity corrected in presence of YFP at the start of the imaging process (before bleaching), and $I_{max}$ is the CFP intensity when CFP reaches its maximal recovery as YFP is totally bleached.

*Single Channel Recording*—HEK293 cells were transfected with pIRES2-EGFP plasmids containing open reading frames of THIK1, THIK2-5RA, and Td-THIK1-THIK2 using Lipofectamine 2000 and OPTI-MEM I reduced serum medium (Life Technologies). Cells were used 2 days after transfection. Electrophysiological recording was performed using a patch clamp amplifier (Axopatch 200B, Molecular Devices). Glass patch pipettes (thick-walled borosilicate, Warner Instruments) coated with SYLGARD were used to minimize background noise. Channel current was filtered at 2 kHz and transferred to a computer using the Digidata 1320 interface at a sampling rate of 20 kHz. Single-channel currents were analyzed with the pClamp program, and the tracings shown in the figures were filtered at 1.2 kHz. For analysis of single-channel currents, the amplitude of each channel was set at ~0.5 pA, and the minimum duration was set at 0.05 ms. In experiments using cell-attached patches, pipette and bath solutions contained (in mM): 150 KCl, 1 $MgCl_2$, 5 EGTA, 10 glucose, and 10 HEPES (pH 7.3). All experiments were performed at room temperature (~25 °C). Differences among groups were analyzed using one-way analysis of variance test with post hoc comparisons using the Tukey's test (SPSS18 software). Significance was set at $p < 0.05$. Data were represented as mean ± S.E.

## RESULTS

*Co-expression of THIK1 and THIK2*—To date, the cellular localization of THIK1 and THIK2 has only been achieved in the kidney. Both subunits have the same localization along the mammalian nephron and collecting duct system (31). Only slight differences in intensity and subcellular distribution were observed (31). This co-localization suggested that THIK1 and THIK2 may form heterodimers. However, another study has reported that co-expression of the silent rat THIK2 with the active rat THIK1 had no effect on the current levels, suggesting that THIK2 was not able to assemble with THIK1 (24). To reassess this result, cRNAs coding for human THIK proteins were synthesized *in vitro* and co-injected in *Xenopus* oocytes. 2 days after injection, currents were recorded using two-electrode voltage clamp. Fig. 1*A* displays the theoretical probability of subunit assembly for ratios 1:1 and 1:3. If THIK1 and THIK2 do not assemble, then the current amplitude should correspond to THIK1 homodimers and should not be affected by the co-expression of the silent THIK2. If THIK1 and THIK2 interact but form inactive heterodimers, only a fraction of THIK1 current should remain after co-expression of THIK2 (25% for the ratio 1:1 and 6.25% for the ratio 1:3). Alternatively, if the THIK1/THIK2 heterodimers have the same properties as the THIK1 homodimers, co-injecting THIK2 should increase the total current. Fig. 1 (*B* and *D*) shows that co-expressing THIK2 with THIK1 has none of the expected effects. Increasing THIK2 cRNA induces a moderate decrease of the current amplitude (Fig. 1*B*). For a ratio of 1:3, a 50% decrease of the current is observed, with a shift from 1.8 ± 0.1 μA at 0 mV for THIK1 alone to 0.8 ± 0.07 μA at 0 mV for THIK1 + THIK2 (Fig. 1, *B* and *D*). To rule out a nonspecific effect related to competition for protein translation or trafficking in oocytes, we co-expressed another $K^+$ channel subunit unlikely to assemble with THIK1. We co-expressed THIK1 and a subunit of the $K_{ir}$ channel family, GIRK2-V188G, that is a constitutively active mutant of GIRK2 (28). THIK1 injected alone generates modest inward currents but strong outward currents, whereas GIRK2 currents are mainly inward as $Mg^{2+}$ and polyamines block $K^+$ exit upon depolarization (Fig. 1*C*). Co-expressing the two subunits elicits currents with combined inward and outward currents similar to the expected sum of THIK1 and GIRK2 currents. We then subtracted the averaged current-potential (*I*-V) relationship of GIRK2 from the *I*-V curve obtained from oocytes co-expressing THIK1 and GIRK2. This calculated THIK1 current was compared with the current measured in oocytes expressing THIK1 alone. Inward current amplitude (at −120 mV) and outward current amplitude (at +60 mV) were not significantly different between the calculated and measured conditions demonstrating that in these experimental conditions, THIK1 current is not affected by the expression of another unrelated membrane protein.

We next tested the effect of THIK2 on THIK1 by keeping constant the quantity of total injected cRNAs. Decreasing THIK1 cRNA (alone or by compensating with GIRK2 cRNA) leads to the expected linear decrease of the current amplitude (Fig. 1*E*). When THIK2 is co-expressed, the decrease of the current amplitude is more important and non-linear, confirming that THIK2 has an effect on THIK1. Together with the previous results, this observation suggests that THIK2 does assemble with THIK1, forming a THIK1/THIK2 heterodimer that is less active than the THIK1 homodimer. The lower activity may be due to differences in channel trafficking to the plasma membrane or in permeation properties.

*Design of THIK1 and THIK2 Dominant Negative Mutants*—To confirm heteromerization of THIK1 and THIK2, we designed a more sensitive test based on the dominant negative action of non-functional subunits. THIK subunits with a loss-

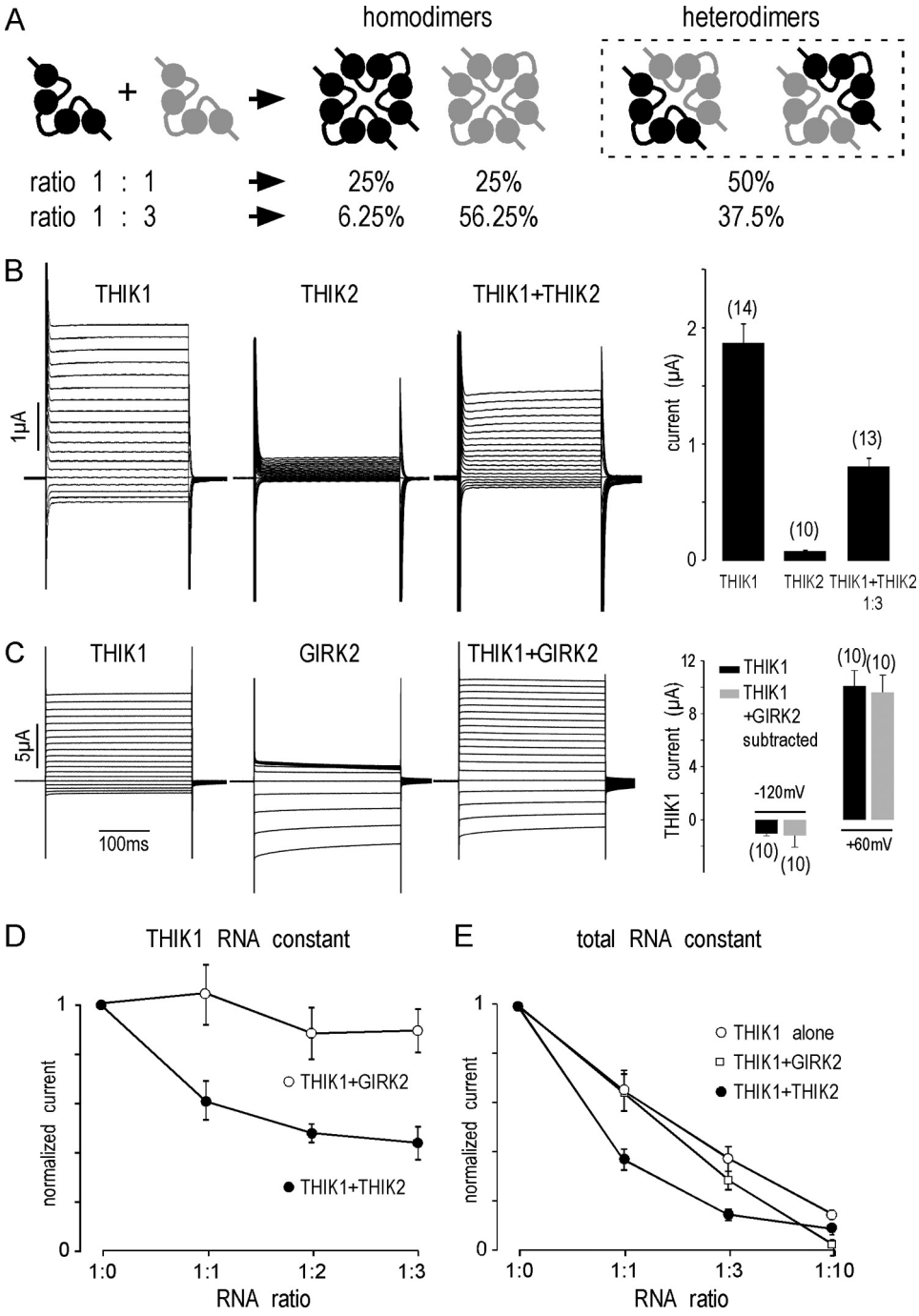


FIGURE 1. **Co-expression of THIK1 and THIK2.** *A*, theoretical probability of dimeric subunit assembly after injection of different ratios of cRNAs. *B*, *left*, representative current traces obtained from oocytes expressing THIK1 (2.5 ng of cRNA/oocyte), THIK2 (7.5 ng of cRNA), or THIK1 and THIK2 (2.5 and 7.5 ng of cRNA, respectively) bathed in ND96 external solution. Currents were recorded at membrane potentials ranging from −120 mV to +60 mV from a holding potential of −80 mV in 10-mV increments. *Right*, histograms representing the steady-state current amplitudes (mean ± S.E.) at 0 mV; the number of oocytes is indicated in *parentheses*. *C*, *left*, representative current traces obtained from oocytes expressing THIK1 (2.5 ng of cRNA/oocyte), GIRK2-V188G (7.5 ng of cRNA), or THIK1 and GIRK2-V188G (2.5 and 7.5 ng of cRNA, respectively) bathed in ND96 external solution. Currents were recorded as in *B*. *Right*, averaged *I*-*V* relationship of GIRK2 was subtracted from the *I*-*V* curve obtained from oocytes co-expressing THIK1 and GIRK2 to obtain a calculated THIK1 current. This calculated THIK1 current (*gray bars*) was compared with the current measured in oocytes expressing THIK1 alone (*black bars*) at −120 mV and at +60 mV. Values represent mean ± S.E.; the number of oocytes is indicated in *parentheses*. *D*, THIK1 cRNA (2.5 ng) was co-injected into oocytes with increasing amounts (0, 2.5, 5 and 7.5 ng) of GIRK2-V188G cRNA (*white circles*) or THIK2 cRNA (*black circles*). The current amplitude at 0 mV for each condition was normalized against the current amplitude measured from oocytes injected with 2.5 ng of THIK1 cRNA. Values represent mean ± S.E. *E*, decreasing amounts of THIK1 cRNA (3, 1.5, 1, and 0.75 ng) were injected alone (*white circles*) or with increasing amounts of THIK2 cRNA (*black circles*) or GIRK2-V188G cRNA (*white squares*) to keep injected cRNAs constant at 3 ng. The current amplitude at 0 mV for each concentration was normalized with THIK1 currents (3 ng).

of-function mutation were designed by replacing the first glycine of the $K^+$ signature sequence (GYG) in the first pore domain (P1) of THIK1 and THIK2 by a glutamate. These mutations are analogous to the G95E mutation in TASK1 and G144E in TREK1 that were previously used to generate dominant negative subunits (32). THIK1-G112E (named $THIK1^{DN}$) and

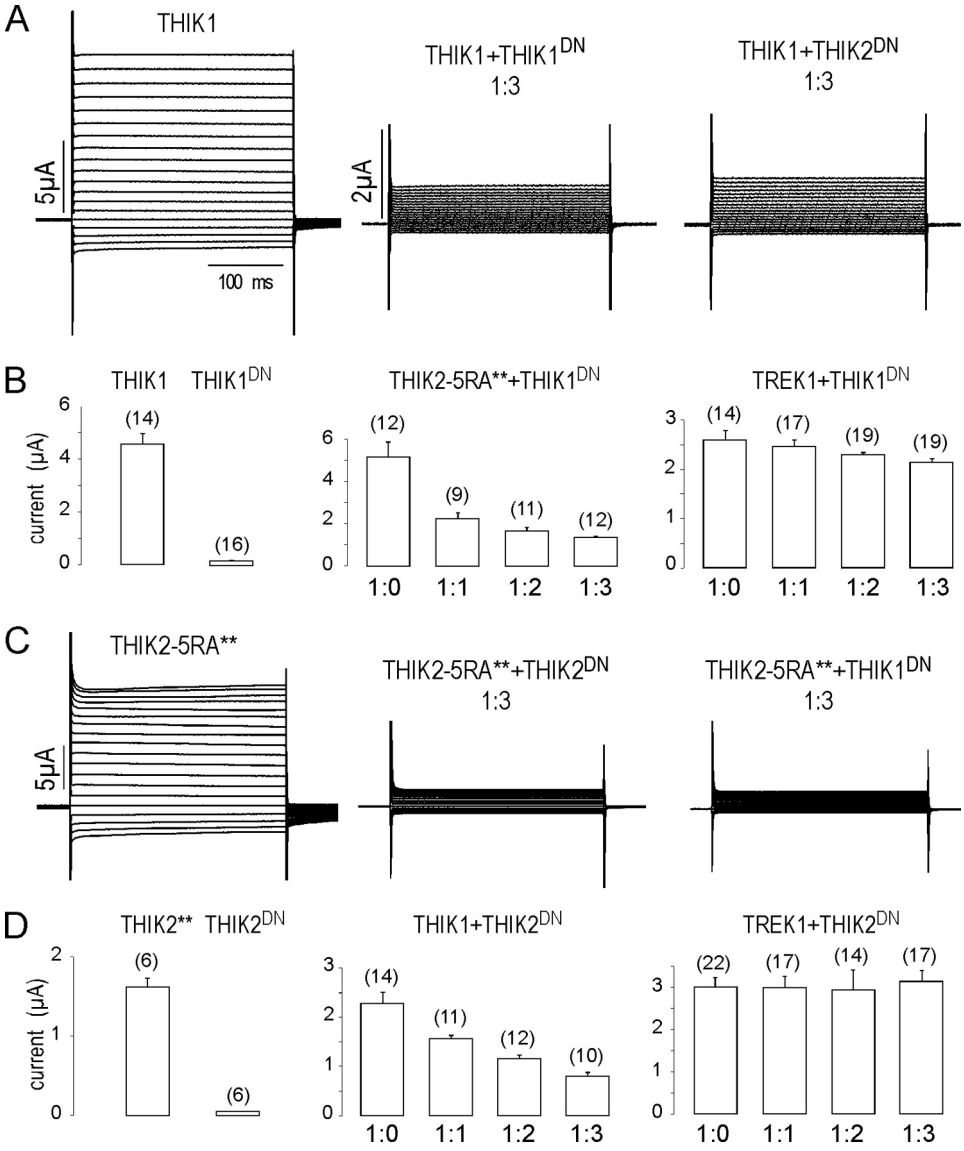


FIGURE 2. **THIK1$^{DN}$ and THIK2$^{DN}$ subunits bearing a loss-of-function mutation act as dominant negatives.** Dominant negative subunits (THIK$^{DN}$) were constructed by mutating a glycine in the $K^+$ signature sequence of the first pore domain (G112E for THIK1 and G131E for THIK2). *A*, representative current traces obtained from oocytes expressing THIK1 (2.5 ng of cRNA/oocyte) in combination with THIK1$^{DN}$ or THIK2$^{DN}$ (7.5 ng of cRNA). Currents were recorded at membrane potentials ranging from −120 mV to +60 mV from a holding potential of −80 mV in 10-mV increments. *B*, histograms representing steady-state average current amplitude (mean ± S.E.) at 0 mV recorded for oocytes expressing THIK1 (2.5 ng of cRNA), THIK2-5RA** (2.5 ng of cRNA), and TREK1 (2.5 ng of cRNA) alone or co-injected with increasing amounts of THIK1$^{DN}$ cRNA (0, 2.5, 5, and 7.5 ng). THIK1$^{DN}$ (7.5 ng of cRNA) expressed alone is a non-functional subunit as illustrated in the *left histogram*. The number of oocytes per condition is indicated in *parentheses*. *C*, representative current traces obtained from oocytes expressing the active mutant THIK2-5RA** alone (2.5 ng of cRNA injected/oocyte) or in combination with THIK1$^{DN}$ or THIK2$^{DN}$ (7.5 ng of cRNA/oocyte). *D*, same experiment as in *B*, but with co-expression of increasing amounts of THIK2$^{DN}$. The number of oocytes per condition is indicated in *parentheses*.

THIK2-G131E (named THIK2$^{DN}$) mutants were expressed in oocytes alone or in combination with their functional homolog subunit (Fig. 2). As expected, when expressed alone, THIK1$^{DN}$ and THIK2$^{DN}$ failed to produce currents (Fig. 2, *B* and *D*). Then we verified that THIK1$^{DN}$ was acting as a dominant negative subunit on THIK1. To favor the formation of inactive THIK1/THIK1$^{DN}$ heterodimers *versus* active THIK1/THIK1 homodimers, we used a ratio of 1:3 between wild-type and loss-of-function subunits (Fig. 2*A*). As expected, THIK1$^{DN}$ was able to inhibit current expression. The suppressing effect was almost complete, as THIK1 current amplitude dropped from 3.5 ± 0.3 µA, $n = 9$ at 0 mV to 0.5 ± 0.04 µA, $n = 8$ in the presence of THIK1$^{DN}$ (as compared with 0.07 ± 0.008 µA, $n = 6$ for non-injected oocytes of the same batch). Because THIK2 does not generate measurable current in oocytes, we took advantage of the active mutant THIK2-5RA** that contains the quintuple trafficking mutation 5RA (R11A,R12A,R14A, R15A,R16A) and the double gating mutation ** (A155P,I158D) (26). As shown in Fig. 2*C*, THIK2$^{DN}$ inhibits THIK2-5RA**, the current amplitude shifting from 5.3 ± 0.6 µA, $n = 12$ at 0 mV to 1.7 ± 0.3 µA, $n = 12$ in the presence of THIK2$^{DN}$.

*THIK1$^{DN}$ and THIK2$^{DN}$ Act as Dominant Negative Subunits in Heteromeric THIK1-THIK2 Channels*—We next tested the effect of THIK1$^{DN}$ on THIK2-5RA** and of THIK2$^{DN}$ on THIK1. The dominant negative effect of the mutated subunits is dose-dependent and maximum at ratio 1:3 (Fig. 2). THIK1$^{DN}$

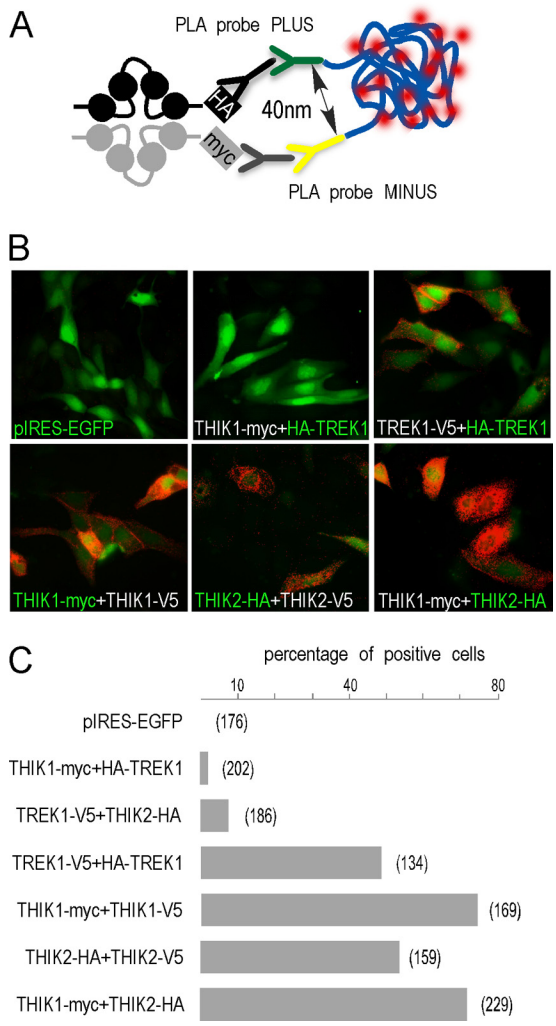


FIGURE 3. **Visualization of the THIK1/THIK2 interaction by *in situ* proximity ligation assay (PLA, Duolink technology).** *A*, schematic description of PLA. *B*, MDCK cells were co-transfected with different combinations of THIK1, THIK2, and TREK1. Subunits were tagged as indicated (Myc, V5, or HA tags), and antibodies directed against these tags were used for PLA. For each test of interaction, one of the two subunits was cloned into a pIRES2-EGFP vector to visualize transfected cells (green cells, the subunit subcloned into pIRES2-EGP is indicated in *green*). *Bright red dots* correspond to positive PLA between interacting subunits. Homodimeric THIK1, THIK2, and TREK1 channels and heterodimeric THIK1/THIK2 channels gave a positive signal. No signal was observed when THIK1 or THIK2 were co-expressed with TREK1. *C*, quantification of the PLA-positive signal. The percentage of cells corresponds to the number of PLA-positive cells (*green* and *red*) relative to the number of transfected cells (*green*). The number of observed cells is indicated in *parentheses*. Each condition was repeated three times.

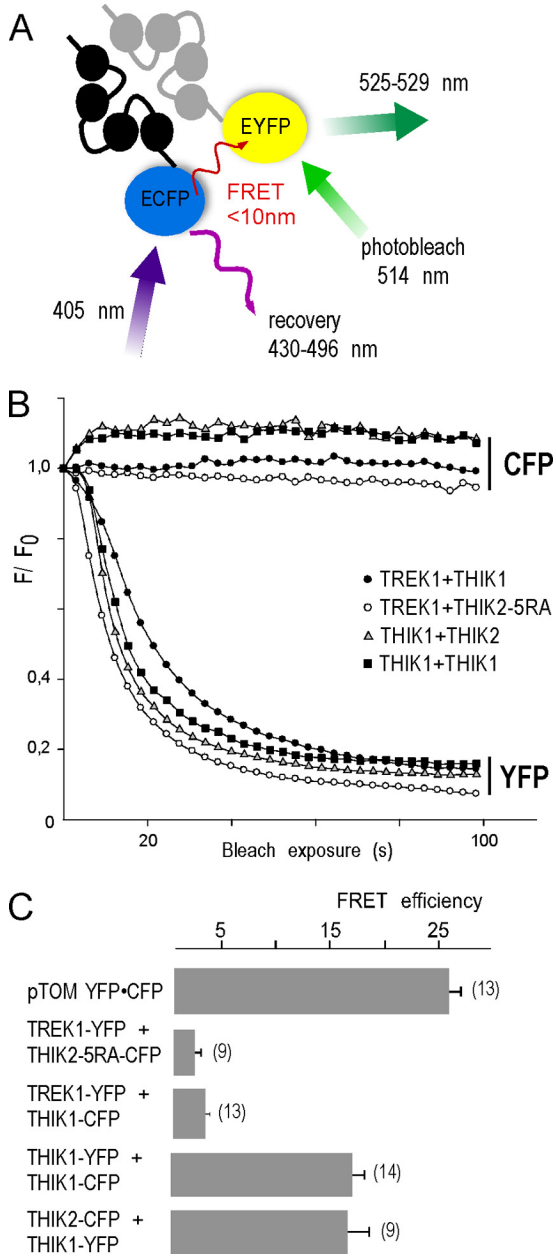


FIGURE 4. **THIK1-THIK2 interaction visualized using FRET technology.** *A*, schematic description of FRET measurement by acceptor bleaching. *B*, FRET measurements. Different combinations of THIK1, THIK2, THIK2-5RA (surface expressed THIK2), and TREK1 subunits fused to EYFP or ECFP were co-transfected in MDCK cells. For FRET positive control condition, pTOM, a plasmid in which EYFP is directly linked to ECFP, was transfected alone. For each condition, FRET was measured at the plasma membrane during a bleach exposure of EYFP (594 nm) while ECFP fluorescence was recovering (407 nm). *F* (fluorescence) over $F_0$ (fluorescence at $t = 0$) was plotted to normalize the intensity and observe CFP recovery, whereas YFP was photobleached. *C*, quantification of the FRET signals (mean ± S.E.). The number of cells per condition is indicated in *parentheses*. Each condition was repeated three times.

largely inhibits THIK2-5RA** (Fig. 2, *A* and *B*), the current measured at 0 mV decreasing from 5.2 ± 0.6 μA, $n = 12$ to 1.3 ± 0.1 μA, $n = 12$ in the presence of $THIK1^{DN}$ (ratio 1:3). Conversely, co-expression of $THIK2^{DN}$ with THIK1 suppresses the expressed current, from 2.3 ± 0.2 μA, $n = 14$ to 0.8 ± 0.08 μA, $n = 10$ (ratio 1:3, Fig. 2, *A* and *D*). As expected, $THIK1^{DN}$ and $THIK2^{DN}$ have no significant effect on the current produced by TREK1, a distant $K_{2P}$ subunit (Fig. 2, *B* and *D*).

*Physical Interaction of THIK1 and THIK2 Subunits*—Assembly of THIK1 and THIK2 was next tested using the Duolink *in situ* PLA and the FRET technology (Figs. 3 and 4). Both techniques rely on the very close proximity between interacting proteins (<40 nm for Duolink PLA and <10 nm for FRET) (Figs. 3*A* and 4*A*). A strong PLA signal corresponding to homodimers was observed in MDCK cells expressing THIK1, THIK2, or TREK1 subunits tagged with two different sequences (Myc, V5, or HA tags). 74.5% of the cells gave positive PLA signal for THIK1 homodimers, and 53.5% gave positive PLA signal for THIK2 homodimer. A strong signal was also observed in 71.6% of the cells co-expressing THIK1 and THIK2, demonstrating the formation of heterodimers (Fig. 3, *B* and *C*).

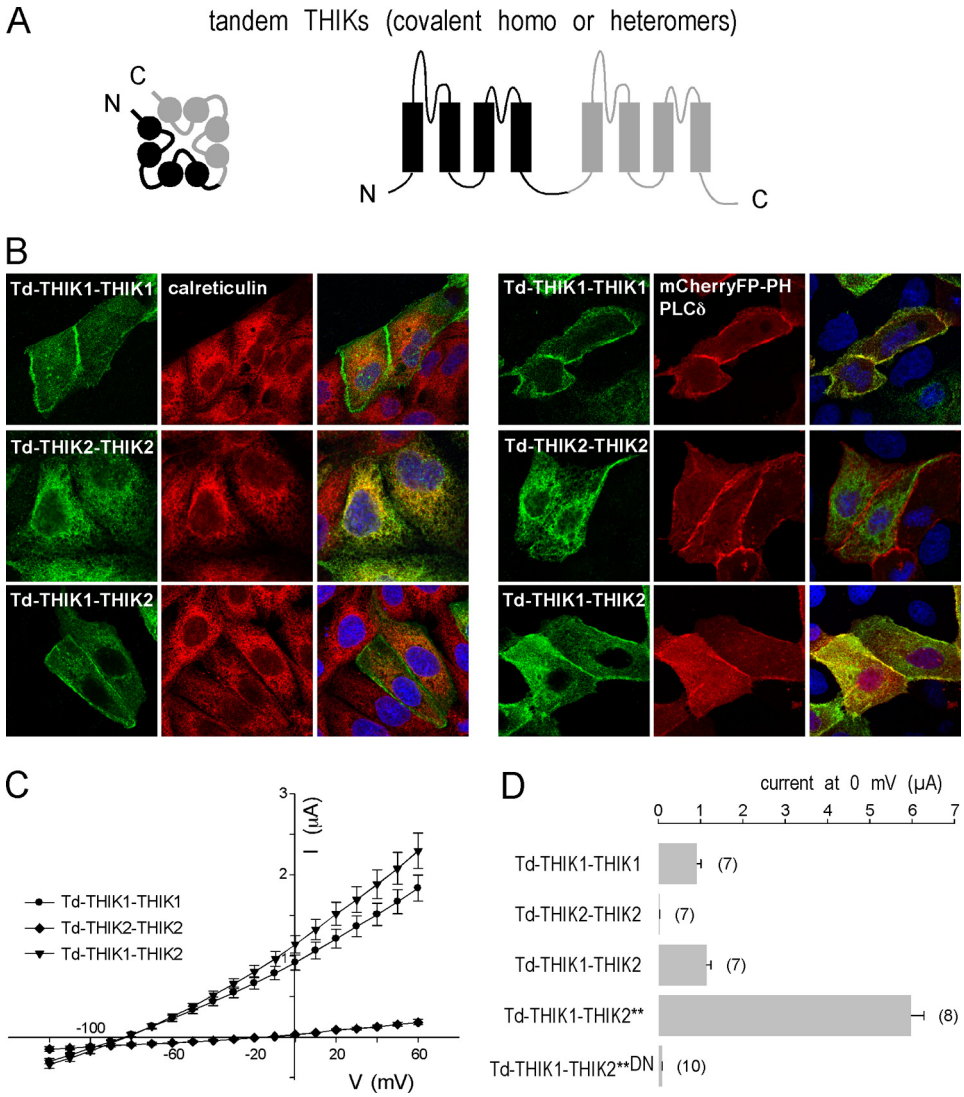


FIGURE 5. **Subcellular distribution and electrophysiology of covalent tandems of THIK subunits (Td-THIK-THIK).** *A*, plasmids expressing covalent dimers were designed by fusing in-frame the sequences coding for THIK1 and THIK2. A tag sequence was introduced at the C-terminal region of the tandem (Myc or HA tags). *N*, N terminus; C, *C* terminus. *B*, subcellular distribution of tandems of THIKs in transfected MDCK cells. Cells were labeled with primary anti-tag antibodies for the detection of the tandems (*green*) and with primary antibodies directed against endogenous calreticulin, a resident protein from the ER, or transfected mCherryFP-PH-PLC∂, a plasma membrane marker (in *red*). *C*, averaged current-voltage (*I-V*) relationships obtained from currents recorded from oocytes injected with 10 ng of Td-THIK1-THIK1-Myc, Td-THIK2-THIK2-HA, or Td-THIK1-THIK2-HA cRNAs. Amplitude values are taken at the steady state of the depolarization pulses and correspond to mean ± S.E., $n = 7$ oocytes/condition. *D*, steady-state current amplitude at 0 mV (mean ± S.E.) for wild-type and mutant homodimeric and heterodimeric tandems. 10 ng of cRNA were injected, and oocytes were recorded 1 day after injection. The number of oocytes per condition is indicated in *parentheses*.

As negative controls, THIK2 and THIK1 were co-expressed with TREK1, a distant $K_{2P}$ subunit (Fig. 3, *B* and *C*). Only 2.4% of the cells co-expressing THIK1 and TREK1 gave a PLA signal, 7.5% for the cells co-expressing THIK2 and TREK1 (Fig. 3*C*). These results were further confirmed by FRET. Different combinations of THIK1, THIK2, THIK2-5RA, and TREK1 fused to EYFP or ECFP were co-transfected in MDCK cells. For each condition, FRET was detected by measuring the increase of CFP donor intensity after photobleaching of EYFP acceptor (Fig. 4*A*) (33). For the FRET positive control condition, pTOM, a plasmid for expression of EYFP directly linked to ECFP, was transfected alone. With this covalent tandem of fluorescent proteins, FRET efficiency was 25.5 ± 1.3%, $n = 13$. Co-transfection of THIK1 and THIK2 generated FRET. The efficiency of 16.6 ± 2%, $n = 9$ is not significantly different from the FRET produced by THIK1 homodimers, 17 ± 1.2%, $n = 14$. TREK1 is not able to generate FRET when co-expressed with THIK1 (2.9 ± 0.4%, $n = 13$) or THIK2-5RA (1.9 ± 0.6%, $n = 9$), confirming the specific assembly of THIK1 with THIK2 (Fig. 4, *B* and *C*).

*Covalent THIK1-THIK2 Tandems Are Present in the Plasma Membrane and Generate $K^+$ Currents*—To verify that heteromeric THIK1-THIK2 channels are functional and produce currents, we prepared plasmids for expression of tandems (named Td-THIKx-THIKx) in which two identical or different subunits are covalently linked (Fig. 5*A*). Unlike co-injection of two different cRNAs that generates a mix of homo- and heterodimeric channels, this technique gives access to pure heteromeric channels. Subcellular distributions of the covalent tandems were compared with the distribution of mCherryFP-PH-PLCδ, a transfected plasma membrane protein, and of calreticulin, an

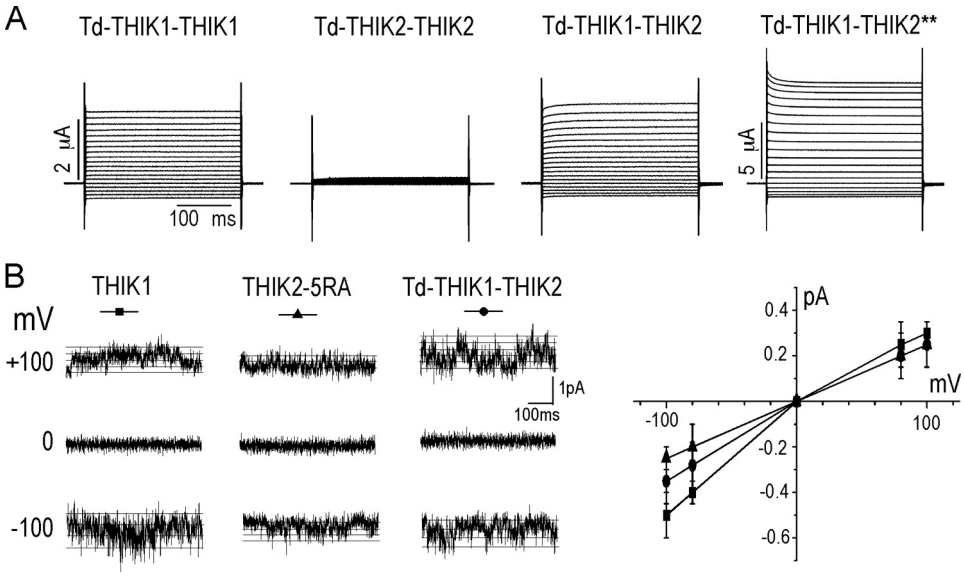


FIGURE 6. **Td-THIK1-THIK2 current and single channel recording.** *A*, THIK1-THIK2 covalent tandems are functional and present intermediate current kinetics. Td-THIK1-THIK1, Td-THIK2-THIK2, Td-THIK1-THIK2, or Td-THIK1-THIK2** tandems were expressed in *Xenopus* oocytes. Currents were recorded at membrane potentials ranging from −120 mV to +60 mV from a holding potential of −80 mV in 10-mV increments. *B*, *left*, single-channel recordings from transfected HEK293 cells expressing THIK1, THIK2-5RA, or Td-THIK1-THIK2. Currents were recorded in cell-attached patches held at pipette potentials of +100 and −100 mV in bath solution containing 150 mM KCl. Channel openings are indicated by *dotted lines*. *Right*, single channel current-voltage relationships of THIK1, THIK2, and Td-THIK1-THIK2. Data are represented as mean ± S.E.

endogenous endoplasmic reticulum (ER) resident protein. Like THIK1 (26), Td-THIK1-THIK1 channels distribute to the cell surface where they strongly co-localize with the plasma membrane fluorescent protein (Fig. 5*B*). Like THIK2 (26), Td-THIK2-THIK2 channels show an intracellular staining that co-localizes with the ER marker (Fig. 5*B*). These results show that the covalent link does not affect the folding, assembly, and trafficking of the homomeric channels in their respective compartments. More interestingly, the heteromeric tandem Td-THIK1-THIK2 is distributed mainly at the plasma membrane, suggesting that the association of THIK1 with THIK2 overcomes the ER retention signal present in THIK2, promoting the recruitment of the heteromeric tandem at the plasma membrane.

To test the functionality of heteromeric channels, we compared the currents produced by Td-THIK1-THIK2 with Td-THIK1-THIK1 and Td-THIK2-THIK2 (Fig. 5, *C* and *D*). Although Td-THIK2-THIK2 does not generate macroscopic currents as expected, both Td-THIK1-THIK1 and Td-THIK1-THIK2 produce $K^+$ currents. These currents are of comparable amplitudes (0.9 ± 0.09 μA, $n = 7$ *versus* 1.1 ± 0.1 μA, $n = 7$ at 0 mV) with similar hyperpolarized reversal potentials (−81.4 ± 2.8 mV *versus* −80.7 ± 2 mV, Fig. 5*C*). Introducing the gating mutations that stimulate THIK2 (A155P,I158D) into Td-THIK1-THIK2 produces a strong current increase (5.9 ± 0.3 μA, $n = 8$, Fig. 5*D*), whereas introducing the dominant negative mutation results in a complete inhibition (0.09 ± 0.05 μA, $n = 10$, Fig. 5*D*). These results show that the current produced by Td-THIK1-THIK2 is generated by ionic pores comprising the pore domains of both THIK1 and THIK2, and not by the association of THIK1 moieties from different Td-THIK1-THIK2.

Interestingly, the currents produced by Td-THIK1-THIK1 and Td-THIK1-THIK2 exhibit different kinetics (Fig. 6*A*). Activation kinetics of Td-THIK1-THIK1 are instantaneous, but are slightly delayed for Td-THIK1-THIK2. Although the current kinetics of Td-THIK1-THIK1 are similar to those of THIK1, the kinetics of Td-THIK1-THIK2 resemble the ones of THIK2-A155P (26). We have shown that the proline mutation is unrelated to these particular kinetics that seem rather characteristics of THIK2 (26). This observation is consistent with the fact that THIK1 and THIK2 form functional heteromultimeric channels with current properties different from homomultimeric THIK1 channels. We also compared kinetics of the currents produced by tandems containing THIK2 and THIK2-A155P-I158D (THIK2**), to take advantage of the dramatic effect of the double mutation on THIK2 channel gating. Tandem channels containing THIK1 linked to either THIK2 or THIK2** generate current with different properties (Fig. 6*A*). Tandems containing THIK2** produce more currents that saturate upon strong depolarizations (Fig. 6*A*). All these results, combined with the effects of the dominant negative subunits, show that in addition to forming homodimeric channels, the two THIK subunits can associate to produce heterodimers with distinct properties.

*Single Channel Properties of Homodimeric and Heterodimeric THIK Channels*—To compare the conductance among THIK1 homodimers, THIK2 homodimers and THIK1/THIK2 heterodimers at the single-channel level, cell-attached patches were formed on HEK293 cells using pipette and bath solutions containing 150 mM KCl. Cells were transfected with THIK1, THIK2-5RA (26), or Td-THIK1-THIK2 for the expression of pure heterodimeric channels. Single-channel openings of THIK channels at −100 mV and +100 mV are shown in Fig. 6*B*. The current-voltage relationship was plotted using the mean amplitude values at different potentials. In agreement with an earlier study (34), cells transfected with THIK-1 showed short and spiky channel opening and a weak inward rectification. The

unitary conductance was ~5 pS. THIK2 also showed small conductance with a noisy open state and a linear relationship between current and voltage. The single-channel conductance was 2.5 ± 1.0 pS, $n = 5$ at −100 mV. The single-channel conductance of THIK1/THIK2 heterodimers was 3.5 ± 0.8 pS, $n = 5$, intermediate between THIK1 and THIK2. THIK channels with short and spiky openings were active at all the membrane potentials tested in this study.

## DISCUSSION

*THIK Subunit Dimerization*—Among the 15 $K_{2P}$ channel subunits, only one example of heteromerization has been extensively documented *in vitro* and *in vivo* that relates to TASK1 and TASK3 subunits (18, 19). Dominant negative subunits have been used to establish the heteromerization of TASK channels in heterologous systems (18, 32). By using the same approach, we were able to reciprocally abolish THIK1 and THIK2 current in *Xenopus* oocytes by using non-conducting $THIK2^{DN}$ and $THIK1^{DN}$ mutants (Fig. 2). In another study, the authors took advantage of the difference in ruthenium red and pH sensitivities between TASK1 and TASK3 subunits to further characterize heterodimeric channels (19). Co-expression of TASK1 and TASK3 yielded currents with pharmacological properties distinct from the linear combinations of TASK1 and TASK3 homodimeric currents. The same features were obtained with tandem constructs in which TASK1 and TASK3 were covalently linked together (19). We previously found that THIK1 and THIK2 channels were insensitive to pH and inhibited to the same extent by halothane (26). In this context, it is not surprising that the co-expression of THIK2 with THIK1 does not affect current characteristic as has been reported earlier (24) (Fig. 1). However, it does not mean that THIK2 cannot be part of the recorded channel. To overcome this limitation, we took advantage of a THIK2 mutant channel (I158D) showing current saturation upon depolarization. We generated covalent tandems of THIK channels to prevent contamination by homomeric channels that would affect analysis of heteromeric channels. This allowed us to record Td-THIK1-THIK2 currents (Fig. 5). Moreover, Td-THIK1-THIK2** produces currents with higher amplitude and intermediate rectification properties (Figs. 5 and 6), whereas Td-THIK1-$THIK2^{**DN}$ had lost its functionality. These results confirm the involvement of THIK2 in the formation of active heteromeric channels. Physical association of THIK subunits was also supported by Duolink *in situ* proximity ligation assay and FRET, two techniques commonly used to visualize two proteins in very close spatial proximity (Figs. 3 and 4).

*Single-channel Properties of THIK Channels*—A recent study has shown that THIK1 has a very small single-channel conductance (~5 pS at +100 mV) and short open time duration (<0.5 ms) (34). Thus, THIK1 was the $K_{2P}$ channel with the smallest unitary conductance reported so far. Here, we show that the conductance of THIK2 is even smaller (~2.5 pS). Interestingly, THIK1-THIK2 heterodimers display an intermediate single-channel conductance of ~3.5 pS. These small unitary conductances are characteristic of THIK currents and should help to identify native THIK currents. However, the slight difference between these single channel conductances may impair the distinction between THIK channels, especially between homodimers and heterodimers. Functional expression of THIK2 and Td-THIK1-THIK2 should help to carry a better characterization of their regulations and pharmacological profiles. Together with the reported differences in current kinetics and single channel properties, these data will be useful to identify the corresponding $K^+$ channels in native cells.

*THIK Channel Trafficking*—The N-terminal region of THIK2 is responsible for intracellular retention of the homomeric channel in the ER. This retention limits the surface expression of THIK2 channel but could also, in the context of heteromerization, impact the trafficking of THIK1 channels. Such negative effect has been reported for $K_{ir}3.3$, which decreases current and surface expression of $K_{ir}3.1$-containing heteromers (35, 36). We have found no major negative effect of THIK2 expression on THIK1. Rather, we observed complete relocalization of THIK2 to the plasma membrane when associated with THIK1 (Fig. 5). Retention due to arginine-based motifs can be masked or unmasked in multimeric channel complexes, controlling composition and stoichiometry of these complexes at the cell surface. For example, $K_{ATP}$ channels are active as an octameric complex consisting of four $K_{ir}$ proteins and four SUR proteins (37–39). Each subunit contains an ER retention motif similar to the one present in THIK2. After complete assembly of the octameric $K_{ATP}$ channel, when all ER retention motifs are shielded by assembling and folding of the multimeric complex, the functional channel reaches the surface and plays its physiological role (40, 41). Because THIK1-THIK2 heterodimers localize at the cell surface in MDCK (Fig. 5*B*) and produce currents in oocytes (Fig. 5*C*), we can speculate that in the tandem, THIK1 masks the ER retention/retrieval motif of THIK2. THIK2 homomultimeric channels are poorly active due to combined intracellular retention and low basal activity. Association with THIK1 relieves ER retention and low intrinsic activity, suggesting that this heteromerization may be the preferred way for THIK2 to exert its function. This may also be true for other silent $K_{2P}$ channels such as KCNK7 and TASK5 for which no current has yet been recorded despite experimental attempts to restore their functionality (42–44). However, because mutations that enhance THIK2 channel activity can generate currents of high amplitude in oocytes expressing THIK2 alone or Td-THIK2-THIK2, and because phosphorylation seems to control THIK2 trafficking (26), THIK2 could also operate as a homomultimeric channel stimulated by signaling pathways that have not been identified yet.

*Functional Significance*—THIK1 and THIK2 have distinct cell and tissue expression patterns. However, overlapping distributions in some tissues suggest *in vivo* formation of functional heterodimers, for instance in the olfactory bulb or hippocampus of adult rat brain (24) and in mouse, rat, and human kidneys (31). Also, changes in the ratio of THIK1 and THIK2 in some tissues or in certain conditions may also significantly influence assembly and composition of THIK channels. Mouse THIK2 transcripts, but not THIK1, are up-regulated specifically in post-migratory cerebellar granule cells during development (45). Similarly, expression of THIK2, but not THIK1, decreases in the cochlear nucleus of a rat model of deafness (46, 47) and in the striatum of chronically nicotine-treated rats (48).

Interestingly, after cutaneous inflammation, THIK1 and THIK2 transcripts are regulated in an opposite manner in rat dorsal root ganglion neurons (49). In all these different conditions, the ratio between homomultimeric and heteromultimeric channels would be influenced by the transcriptional regulation of each THIK subunit. In specific tissues and/or upon specific regulation, the cell may favor formation of homomultimeric or heteromultimeric THIK channels providing an additional diversity of $K^+$ currents.

*Acknowledgments—We thank Maud Larroque for excellent technical assistance in molecular biology, Nathalie Leroudier for assistance in sequencing analysis, and Frederic Brau for support in confocal microscopy and FRET experiments. We also thank Amanda Patel for the generous gift of pIRES-EGFP and TREK1-EYFP plasmids and Arnaud Echard and Franck Perez for the gift of mCherryFP-PH PLCδ.*

## REFERENCES


1. Coetzee, W. A., Amarillo, Y., Chiu, J., Chow, A., Lau, D., McCormack, T., Moreno, H., Nadal, M. S., Ozaita, A., Pountney, D., Saganich, M., Vega-Saenz de Miera, E., and Rudy, B. (1999) Molecular diversity of $K^+$ channels. *Ann. N.Y. Acad. Sci.* **868,** 233–285
2. Catterall, W. A. (1995) Structure and function of voltage-gated ion channels. *Annu. Rev. Biochem.* **64,** 493–531
3. Hibino, H., Inanobe, A., Furutani, K., Murakami, S., Findlay, I., and Kurachi, Y. (2010) Inwardly rectifying potassium channels: their structure, function, and physiological roles. *Physiol. Rev.* **90,** 291–366
4. Lesage, F., Reyes, R., Fink, M., Duprat, F., Guillemare, E., and Lazdunski, M. (1996) Dimerization of TWIK-1 $K^+$ channel subunits via a disulfide bridge. *EMBO J.* **15,** 6400–6407
5. Lopes, C. M., Zilberberg, N., and Goldstein, S. A. (2001) Block of Kcnk3 by protons: evidence that 2-P-domain potassium channel subunits function as homodimers. *J. Biol. Chem.* **276,** 24449–24452
6. Isacoff, E. Y., Jan, Y. N., and Jan, L. Y. (1990) Evidence for the formation of heteromultimeric potassium channels in *Xenopus* oocytes. *Nature* **345,** 530–534
7. Sheng, M., Liao, Y. J., Jan, Y. N., and Jan, L. Y. (1993) Presynaptic A-current based on heteromultimeric $K^+$ channels detected *in vivo*. *Nature* **365,** 72–75
8. Wang, H., Kunkel, D. D., Martin, T. M., Schwartzkroin, P. A., and Tempel, B. L. (1993) Heteromultimeric $K^+$ channels in terminal and juxtaparanodal regions of neurons. *Nature* **365,** 75–79
9. Yang, W. P., Levesque, P. C., Little, W. A., Conder, M. L., Ramakrishnan, P., Neubauer, M. G., and Blanar, M. A. (1998) Functional expression of two KvLQT1-related potassium channels responsible for an inherited idiopathic epilepsy. *J. Biol. Chem.* **273,** 19419–19423
10. Duprat, F., Lesage, F., Guillemare, E., Fink, M., Hugnot, J. P., Bigay, J., Lazdunski, M., Romey, G., and Barhanin, J. (1995) Heterologous multimeric assembly is essential for $K^+$ channel activity of neuronal and cardiac G-protein-activated inward rectifiers. *Biochem. Biophys. Res. Commun.* **212,** 657–663
11. Kofuji, P., Davidson, N., and Lester, H. A. (1995) Evidence that neuronal G-protein-gated inwardly rectifying $K^+$ channels are activated by $G\beta\gamma$ subunits and function as heteromultimers. *Proc. Natl. Acad. Sci. U.S.A.* **92,** 6542–6546
12. Lesage, F., Guillemare, E., Fink, M., Duprat, F., Heurteaux, C., Fosset, M., Romey, G., Barhanin, J., and Lazdunski, M. (1995) Molecular properties of neuronal G-protein-activated inwardly rectifying $K^+$ channels. *J. Biol. Chem.* **270,** 28660–28667
13. Krapivinsky, G., Gordon, E. A., Wickman, K., Velimirović, B., Krapivinsky, L., and Clapham, D. E. (1995) The G-protein-gated atrial $K^+$ channel IKACh is a heteromultimer of two inwardly rectifying $K^+$-channel proteins. *Nature* **374,** 135–141
14. Liao, Y. J., Jan, Y. N., and Jan, L. Y. (1996) Heteromultimerization of G-protein-gated inwardly rectifying $K^+$ channel proteins GIRK1 and GIRK2 and their altered expression in weaver brain. *J. Neurosci.* **16,** 7137–7150
15. Enyedi, P., and Czirják, G. (2010) Molecular background of leak $K^+$ currents: two-pore domain potassium channels. *Physiol. Rev.* **90,** 559–605
16. Chatelain, F. C., Bichet, D., Douguet, D., Feliciangeli, S., Bendahhou, S., Reichold, M., Warth, R., Barhanin, J., and Lesage, F. (2012) TWIK1, a unique background channel with variable ion selectivity. *Proc. Natl. Acad. Sci. U.S.A.* **109,** 5499–5504
17. Noël, J., Sandoz, G., and Lesage, F. (2011) Molecular regulations governing TREK and TRAAK channel functions. *Channels (Austin)* **5,** 402–409
18. Berg, A. P., Talley, E. M., Manger, J. P., and Bayliss, D. A. (2004) Motoneurons express heteromeric TWIK-related acid-sensitive $K^+$ (TASK) channels containing TASK-1 (KCNK3) and TASK-3 (KCNK9) subunits. *J. Neurosci.* **24,** 6693–6702
19. Czirják, G., and Enyedi, P. (2002) Formation of functional heterodimers between the TASK-1 and TASK-3 two-pore domain potassium channel subunits. *J. Biol. Chem.* **277,** 5426–5432
20. Plant, L. D., Zuniga, L., Araki, D., Marks, J. D., and Goldstein, S. A. (2012) SUMOylation silences heterodimeric TASK potassium channels containing K2P1 subunits in cerebellar granule neurons. *Sci. Signal.* **5,** ra84
21. Feliciangeli, S., Bendahhou, S., Sandoz, G., Gounon, P., Reichold, M., Warth, R., Lazdunski, M., Barhanin, J., and Lesage, F. (2007) Does sumoylation control K2P1/TWIK1 background $K^+$ channels? *Cell* **130,** 563–569
22. Rajan, S., Plant, L. D., Rabin, M. L., Butler, M. H., and Goldstein, S. A. (2005) Sumoylation silences the plasma membrane leak $K^+$ channel K2P1. *Cell* **121,** 37–47
23. Hwang, E. M., Kim, E., Yarishkin, O., Woo, D. H., Han, K. S., Park, N., Bae, Y., Woo, J., Kim, D., Park, M., Lee, C. J., and Park, J. Y. (2014) A disulphide-linked heterodimer of TWIK-1 and TREK-1 mediates passive conductance in astrocytes. *Nat. Commun.* **5,** 3227
24. Rajan, S., Wischmeyer, E., Karschin, C., Preisig-Müller, R., Grzeschik, K. H., Daut, J., Karschin, A., and Derst, C. (2001) THIK-1 and THIK-2, a novel subfamily of tandem pore domain $K^+$ channels. *J. Biol. Chem.* **276,** 7302–7311
25. Girard, C., Duprat, F., Terrenoire, C., Tinel, N., Fosset, M., Romey, G., Lazdunski, M., and Lesage, F. (2001) Genomic and functional characteristics of novel human pancreatic 2P domain $K^+$ channels. *Biochem. Biophys. Res. Commun.* **282,** 249–256
26. Chatelain, F. C., Bichet, D., Feliciangeli, S., Larroque, M. M., Braud, V. M., Douguet, D., and Lesage, F. (2013) Silencing of the tandem pore domain halothane-inhibited $K^+$ channel 2 (THIK2) relies on combined intracellular retention and low intrinsic activity at the plasma membrane. *J. Biol. Chem.* **288,** 35081–35092
27. Renigunta, V., Zou, X., Kling, S., Schlichthörl, G., and Daut, J. (2014) Breaking the silence: functional expression of the two-pore-domain potassium channel THIK-2. *Pflugers Arch.* **466,** 1735–1745
28. Yi, B. A., Lin, Y. F., Jan, Y. N., and Jan, L. Y. (2001) Yeast screen for constitutively active mutant G protein-activated potassium channels. *Neuron* **29,** 657–667
29. Van Munster, E. B., Kremers, G. J., Adjobo-Hermans, M. J., and Gadella, T. W., Jr. (2005) Fluorescence resonance energy transfer (FRET) measurement by gradual acceptor photobleaching. *J. Microsc.* **218,** 253–262
30. Schneider, C. A., Rasband, W. S., and Eliceiri, K. W. (2012) NIH Image to ImageJ: 25 years of image analysis. *Nat. Methods* **9,** 671–675
31. Theilig, F., Goranova, I., Hirsch, J. R., Wieske, M., Unsal, S., Bachmann, S., Veh, R. W., and Derst, C. (2008) Cellular localization of THIK-1 ($K_{2P}$13.1) and THIK-2 ($K_{2P}$12.1) $K^+$ channels in the mammalian kidney. *Cell. Physiol. Biochem.* **21,** 63–74
32. Lauritzen, I., Zanzouri, M., Honoré, E., Duprat, F., Ehrengruber, M. U., Lazdunski, M., and Patel, A. J. (2003) $K^+$-dependent cerebellar granule neuron apoptosis. Role of task leak $K^+$ channels. *J. Biol. Chem.* **278,** 32068–32076
33. Karpova, T., and McNally, J. G. (2006) Detecting protein-protein interactions with CFP-YFP FRET by acceptor photobleaching. in *Current Protocols in Cytometry*, Chapter 12, Unit 12.17, John Wiley & Sons, Inc., New York
34. Kang, D., Hogan, J. O., and Kim, D. (2014) THIK-1 ($K_{2P}$13.1) is a small-conductance background $K^+$ channel in rat trigeminal ganglion neurons.

*Pflugers Arch* **466,** 1289–1300
35. Wischmeyer, E., Döring, F., Wischmeyer, E., Spauschus, A., Thomzig, A., Veh, R., and Karschin, A. (1997) Subunit interactions in the assembly of neuronal Kir3.0 inwardly rectifying $K^+$ channels. *Mol. Cell. Neurosci.* **9,** 194–206
36. Ma, D., Zerangue, N., Raab-Graham, K., Fried, S. R., Jan, Y. N., and Jan, L. Y. (2002) Diverse trafficking patterns due to multiple traffic motifs in G protein-activated inwardly rectifying potassium channels from brain and heart. *Neuron* **33,** 715–729
37. Clement, J. P., 4th, Kunjilwar, K., Gonzalez, G., Schwanstecher, M., Panten, U., Aguilar-Bryan, L., and Bryan, J. (1997) Association and stoichiometry of $K_{ATP}$ channel subunits. *Neuron* **18,** 827–838
38. Inagaki, N., Gonoi, T., and Seino, S. (1997) Subunit stoichiometry of the pancreatic $\beta$-cell ATP-sensitive $K^+$ channel. *FEBS Lett.* **409,** 232–236
39. Shyng, S., and Nichols, C. G. (1997) Octameric stoichiometry of the $K_{ATP}$ channel complex. *J. Gen. Physiol.* **110,** 655–664
40. Schwappach, B., Zerangue, N., Jan, Y. N., and Jan, L. Y. (2000) Molecular basis for $K_{ATP}$ assembly: transmembrane interactions mediate association of a $K^+$ channel with an ABC transporter. *Neuron* **26,** 155–167
41. Zerangue, N., Schwappach, B., Jan, Y. N., and Jan, L. Y. (1999) A new ER trafficking signal regulates the subunit stoichiometry of plasma membrane $K_{ATP}$ channels. *Neuron* **22,** 537–548
42. Ashmole, I., Goodwin, P. A., and Stanfield, P. R. (2001) TASK-5, a novel member of the tandem pore $K^+$ channel family. *Pflugers Arch.* **442,** 828–833
43. Kim, D., and Gnatenco, C. (2001) TASK-5, a new member of the tandem-pore $K^+$ channel family. *Biochem. Biophys. Res. Commun.* **284,** 923–930
44. Salinas, M., Reyes, R., Lesage, F., Fosset, M., Heurteaux, C., Romey, G., and Lazdunski, M. (1999) Cloning of a new mouse two-P domain channel subunit and a human homologue with a unique pore structure. *J. Biol. Chem.* **274,** 11751–11760
45. Aller, M. I., and Wisden, W. (2008) Changes in expression of some two-pore domain potassium channel genes (*KCNK*) in selected brain regions of developing mice. *Neuroscience* **151,** 1154–1172
46. Cui, Y. L., Holt, A. G., Lomax, C. A., and Altschuler, R. A. (2007) Deafness associated changes in two-pore domain potassium channels in the rat inferior colliculus. *Neuroscience* **149,** 421–433
47. Holt, A. G., Asako, M., Duncan, R. K., Lomax, C. A., Juiz, J. M., and Altschuler, R. A. (2006) Deafness associated changes in expression of two-pore domain potassium channels in the rat cochlear nucleus. *Hear. Res.* **216–217,** 146–153
48. Yeom, M., Shim, I., Lee, H. J., and Hahm, D. H. (2005) Proteomic analysis of nicotine-associated protein expression in the striatum of repeated nicotine-treated rats. *Biochem. Biophys. Res. Commun.* **326,** 321–328
49. Marsh, B., Acosta, C., Djouhri, L., and Lawson, S. N. (2012) Leak $K^+$ channel mRNAs in dorsal root ganglia: relation to inflammation and spontaneous pain behaviour. *Mol Cell. Neurosci.* **49,** 375–386